



# METHODOLOGICAL PROPOSAL FOR THE DESIGN AND ANALYSIS OF A FORMULA SAE MONOCOQUE

## PROPUESTA METODOLÓGICA PARA EL DISEÑO Y ANÁLISIS DE UN MONOCASCO FORMULA STUDENT

Rafael Wilmer Contreras Urgilés<sup>1,\*</sup> , Carlos Ayrton Jaramillo Andrade<sup>1</sup> ,  
Erick Josué Pizarro Barrera<sup>1</sup> 

Received: 11-04-2021, Received after review: 19-04-2023, Accepted: 05-05-2023, Published: 01-07-2023

### Abstract

This paper explains the methodology employed to design a Formula Student monocoque based on the regulations set forth in 2020. The values obtained from CAD (Computer Aided Design) modeling and FEM (Finite Element Method) analysis are the pillars of this study. The values of mass, center of gravity, and geometry have been specifically selected because they provide crucial information that aids in the identification of optimization points during the design process. The FEM analysis establishes the allowable stresses for the monocoque within the safety parameters, with a minimum admissible safety factor of 1.1. Two CFRP laminates (Carbon Fiber Laminate and Epoxy Resin Laminate) are developed from the model obtained. The first one yields a simulated weight of 38 kg, and the second one a weight of 20 kg. A stress analysis was performed on the lighter-weight model, obtaining results superior to those of a tubular chassis. A 2017 electric single-seater model is taken as a reference.

**Keywords:** Monocoque, FEM, FSAE, center of gravity, CFRP, AEF

### Resumen

En el presente documento se realiza la explicación de la metodología utilizada para el diseño de un monocoque Formula Student basado en el reglamento del año 2020. Los valores obtenidos del modelado mediante software CAD (diseño asistido por computador) y el análisis por MEF (método de elementos finitos) sirven de base para este estudio. Los valores de masa, centro de gravedad y la geometría son los seleccionados, ya que aportan una mayor información, lo que ayuda a determinar puntos de optimización en el proceso de diseño. En el análisis MEF se determina los esfuerzos admisibles por el monocoque y que se encuentran dentro de los parámetros de seguridad, siendo el factor de seguridad mínimo admisible de 1,1. Del modelo obtenido se desarrolla dos laminados CFRP (laminado de fibra de carbono y resina epoxi) de los cuales el primero da un resultado de peso simulado de 38 kg, y la segunda configuración de laminado un resultado de 20 kg. Se somete el modelo con menor peso al análisis de esfuerzos, los resultados obtenidos son superiores a un chasis tubular, se toma como referencia un modelo monoplaça eléctrica del 2017.

**Palabras clave:** monocoque, MEF, FSAE, centro de gravedad, CFRP, AEF

---

<sup>1,\*</sup>Ingeniería Mecánica Automotriz, Universidad Politécnica Salesiana, Cuenca, Ecuador.  
Corresponding author ✉: rcontreras@ups.edu.ec.

Suggested citation: Contreras Urgilés, R. W.; Jaramillo Andrade, C. A. and Pizarro Barrera, E. J. "Methodological Proposal for the Design and Analysis of a Formula SAE Monocoque," *Ingenius, Revista de Ciencia y Tecnología*, N.º 30, pp. 42-53, 2023, DOI: <https://doi.org/10.17163/ings.n30.2023.04>.

## 1. Introduction

The monocoque is a structure that significantly reduces the weight of a vehicle. This chassis is used in elite automobile competitions, like Formula 1, and its subcategories, like Le Mans and Indycar. In Formula 3 tests, established by the International Automobile Federation (FIA), the monocoque is designed to pass static tests considered the desired standard of structural integrity for a monocoque [1].

The materials most commonly used in the manufacturing of monocoques are primarily composed of carbon fiber-reinforced polymer (CFRP) [2] and Honeycomb panels [3]. These materials exhibit high resistance to torsion and stresses and can be formed in almost any geometry. Ashby's research [4] presents a methodological proposal with a sandwich panel composed of three main elements: a core, a matrix, and carbon fiber. The carbon fiber has been studied in different orientations and combinations in the plane [5]. The combinations among degrees have allowed obtaining the desired mechanical properties in different directions and orientations. In the case of Honeycomb, as indicated in the study by Eurenus et al. [6], a symmetric hexagonal pattern of this structure exhibits relatively high properties in terms of compression and resistance to rupture while maintaining low density.

However, these materials have the disadvantage of being expensive and requiring complex manufacturing processes. In the design process, different geometries are considered. The Politécnico di Torino has analyzed different types of models [7, 8], as this parameter is crucial in optimizing the weight of the monocoque [9]. Based on this information, a CAD model that meets all the geometric requirements specified in the FSAE regulations was developed [10, 11]. Regarding chassis manufacturing, the study conducted by [12] has applied a methodology including design, analysis, and subsequent fabrication. The authors have confirmed the reliability of this methodology through dynamic tests.

In this work, geometry and aerodynamics are considered to take advantage of the shape of the monocoque to effectively minimize the need for additional elements that increase its weight [13]. Another significant parameter is the application of the CFRP laminate as an optimization point, as using different laminates can also reduce the overall weight of the vehicle. Additionally, the directions of the fibers help to reinforce some of the stresses to which the structure is subjected [14]. These cutting-edge materials and manufacturing processes optimize and improve performance in automobile competitions [15]. The results of proper lamination and optimal material selection enable the creation of a specific FEM model that, with reduced weight, can withstand the minimum stresses required by the competition [16].

Zhao [17] has studied a specific software used for FEM models, obtaining favorable results in predicting the overall behavior of the model's structure. Regarding the meshing of the model, a suitable element size was selected to create an accurate mathematical model for stress analysis. The most significant stresses applied to the structure are torsional rigidity, longitudinal rigidity, and lateral impact analysis [8]. Considering the design of the monocoque from Squadra Corse Polito [7] and the design from the University of Seville [18], an expected weight optimization of approximately 50% is anticipated. This will result in a more efficient model with reduced weight and a more resistant structure capable of withstanding the stresses applied to these vehicles.

## 2. Materials and Methods

This section presents aspects related to material selection, the main configuration of the panel, and the parameters for developing the design. Furthermore, it describes the results obtained from stress simulation.

### 2.1. Methodology

After analyzing the state of the art, a workflow was developed to determine the order and activities related to the design, structural analysis, and weight optimization of the model.

In the first stage, the FSAE regulations were reviewed to determine the most significant parameters regarding the design and restrictions of the monocoque [11].

In the second stage, the model was designed considering the restrictions previously analyzed [12].

Figure 1 illustrates the complete model. In the third stage, CFRP lamination was conducted to establish the thickness of the final model. The laminate varies depending on the section, as each requires a distinct thickness to withstand the stresses.

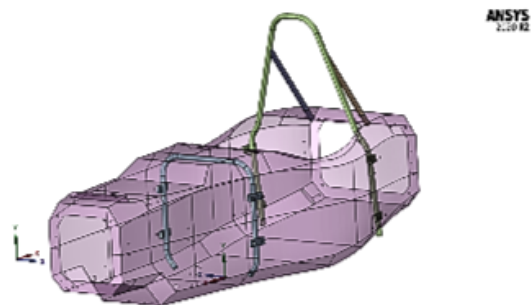


Figure 1. Final surface model

The analysis of the results is presented in detail in the section corresponding to the development of the proposed methodology.

## 2.2. Materials

The materials used in the analysis are carbon fiber fabric reinforcements in a sandwich structure (Figure 2) with Honeycomb. The combination of different materials is known as composite materials. These materials exhibit high mechanical resistance to withstand stresses and excellent stress dissipation capability throughout the structure. This sandwich panel comprises three main components: a core, a matrix, and carbon fibers [4].

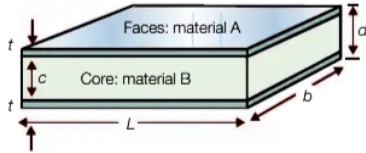


Figure 2. Typical sandwich structure [4]

These materials provide a considerable advantage in terms of overall weight. Their utilization is highly advantageous in constructing a structure with a rigidity comparable to that of a conventional metal structure while reducing its weight by half [5].

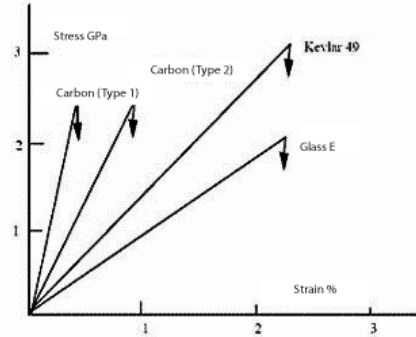


Figure 3. Fiber stress-strain diagram [5]

### 2.2.1. Fibers

Elements made of fiber composite materials can be designed to suit each load case, allowing the material to be created based on specific static requirements. The directions of the fibers can also be customized. The material acquires the desired properties in all orientations by arranging carbon fiber sheets in various directions. The fiber orientations in the plane are  $0^\circ$ ,  $90^\circ$ , and  $\pm 45^\circ$  [5].

Figure 3 demonstrates that Kevlar fiber is the most resistant, whereas carbon fiber is the most rigid. Fiberglass is the least resistant and rigid but is the cheapest of the three.

### 2.2.2. Matrix

The matrix is the material that supports and bonds all the fibers together. The fibers are impregnated into the matrix to form a single material.

Currently, two main types of resins are primarily used for the matrix: epoxy and polyester. Both resins are thermally stable, which means they do not melt under heat, although they may lose some rigidity properties. Additionally, they exhibit an isotropic structural behavior, indicating that their physical properties are similar in all directions. In this study, an epoxy resin was employed.

Table 1 lists some properties of the resins.

Table 1. Resin properties [5]

| Property                                 | Units                    | Epoxy resins | Polyester resins |
|--|--------------------------|--------------|------------------|
| Density                                  | $Mg\ m^{-3}$             | 1.1-1.4      | 1.2-1.5          |
| Young's modulus                          | GPa                      | 3-6          | 2-4.5            |
| Poisson Coefficient                      |                          | 0.38-0.4     | 0.37-0.39        |
| Tensile resistance                       | MPa                      | 35-100       | 40-90            |
| Compression resistance                   | MPa                      | 100-200      | 90-250           |
| Elongation at break (tensile)            | %                        | 1-6          | 2                |
| Thermal conductivity                     | $Wm^{-1}\ C^{-1}$        | 0.1          | 0.2              |
| Expansion Coefficient                    | $10^{-6}\ ^\circ C^{-1}$ | 60           | 100-200          |
| Distortion temperature                   | $^\circ C$               | 50-300       | 50-110           |
| Curing shrinkage                         | %                        | 1-2          | 4-8              |
| Water absorption (24 h a 20 $^\circ C$ ) | %                        | 0.1-0.4      | 0.1-0.3          |

### 2.2.3. Honeycomb Core

There are various types of Honeycomb cores, each with different properties depending on the material used for fabrication. The most common ones are made from aluminum, aramid paper (Nomex), steel, fiberglass, carbon, or ceramic [14]. The Honeycomb core is composed of a symmetrical hexagonal pattern, as depicted in Figure 4. This structure offers excellent compressive and tensile resistance properties and a low density [6].

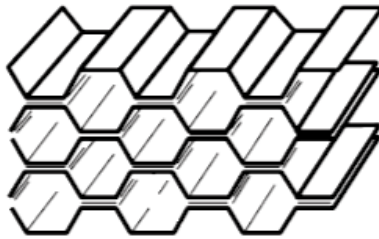


Figure 4. Structure with hexagonal cells [6]

In this study, an aluminum Honeycomb core was selected. This core has an excellent energy absorption capacity, and its thickness is 20 mm.

## 3. Results and discussion

In this section, weight and optimization objectives are established. To achieve a solid theoretical foundation, the flowchart presented in Figure 5 was considered to determine the final model [15].

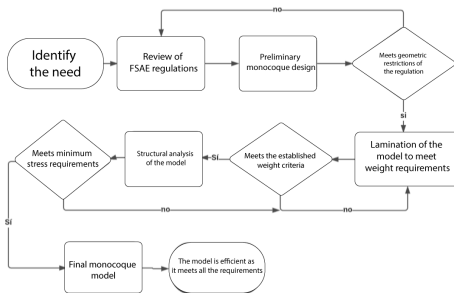


Figure 5. Monocoque design process

### 3.1. Determination of the CAD model

The model's design is based on the regulations for the 95th percentile male, as detailed below:

To maximize driver comfort, various factors are considered, including the vertical and horizontal position of the steering wheel, seat angle, pedal placement, and safety bars [9]. Figure 6 shows the template for the 95th percentile male. The specific distance values are detailed in the FSAE regulations [11]

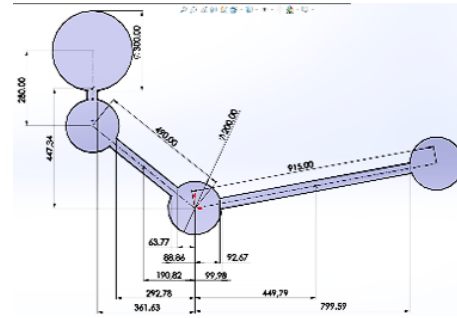


Figure 6. Template for the 95th percentile male [15]

After determining the percentiles and minimum dimensions of the cabin opening, and the minimum cross-sectional area, the first dimensioning is carried out to establish the foundation of the monocoque design. Figure 7 presents the cross-sectional and cabin openings.

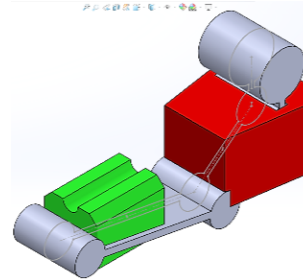


Figure 7. Isometric perspective view of the internal cross-sectional opening [15]

The dimensions of these sections are detailed below: Cabin opening (Figure 8)

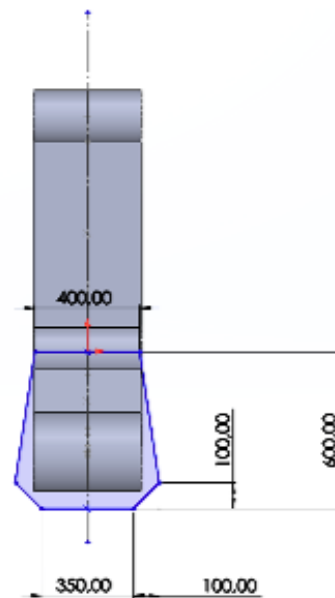
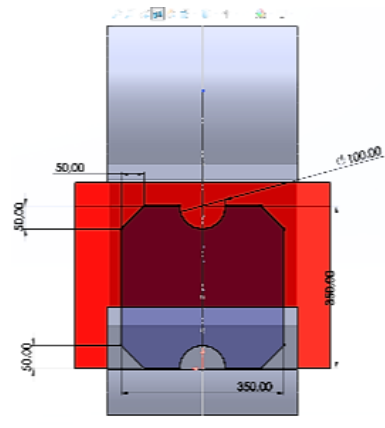


Figure 8. Cabin opening dimensions [15]

- 320 mm above the lowest point of the upper floor surface for monocoque design.
- 400 mm front width.
- 350 mm rear width.
- 600 mm minimum cabin length.

Internal cross-sectional area (Figure 9)



**Figure 9.** Dimensions of the internal cross-sectional area [15]

- An internal cross-sectional area must be kept clear to allow the passage of the template shown through the cabin.
- Minimum length and width of 350 mm.
- Radius of 50 mm at the top and bottom centers.

Using these measurements, a model is created incorporating the main components of the monocoque. These components include a battery located in the rear, an inverter positioned beneath the driver’s legs, and a pair of firewalls. Figure 10 displays the primary side view sketch.

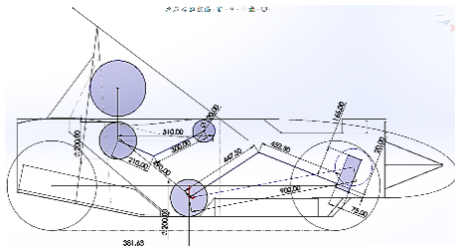


**Figure 10.** Arrangement of components and side sketch [15]

Based on this sketch, the CAD model is created, placing the attachment points of some elements on the monocoque. Figure [11] illustrates the final design.

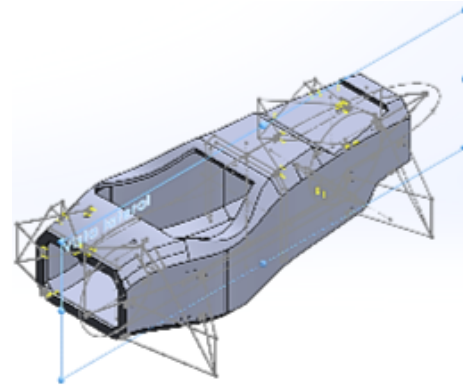


**Figure 11.** Final design of the monocoque [15]

With the final model, the center of gravity and the stresses are obtained, as detailed below:

### 3.2. Determination of the center of gravity

In this section, the weights are applied to the monocoque in the software. Subsequently, the main components selected for calculation are assembled, as shown in Table 2. Using the physical properties tool, the position of the center of gravity of the assembled prototype is determined, as shown in Figure 12.

**Table 2.** Approximate vehicle masses [10]

| Components       | Mass (kg)  | %          |
|------------------|------------|------------|
| Driver           | 70         | 42.85      |
| Battery          | 36         | 20.57      |
| Inverter         | 7          | 4          |
| Pedal box        | 4.5        | 2.57       |
| Steering         | 12.5       | 7.15       |
| Monocoque        | 20         | 11.43      |
| Other components | 20         | 11.43      |
| <b>Total</b>     | <b>175</b> | <b>100</b> |

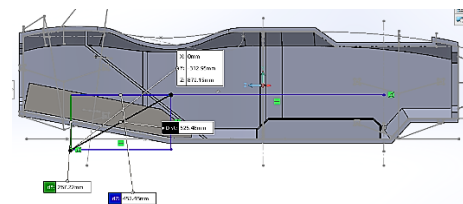


**Figure 12.** Center of gravity location [15]

### 3.3. Lateral mass transfer

To perform this calculation, it is considered that the vehicle follows a curve, acting on the center of gravity with a centrifugal acceleration of 4G. Figure 13 illustrates the free-body diagram defining the center of gravity and the direction of the loads.

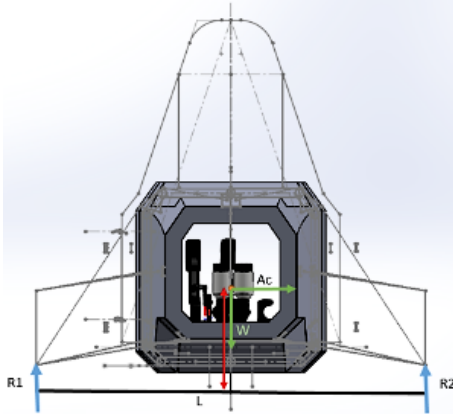


Figure 13. Free body diagram [15]

The R2 reaction is the load that influences torsional rigidity. This torque is applied in opposite directions on both sides of the front axle. A value of 6870 N was used to simulate a higher load on the monocoque and demonstrate the material's stiffness [11].

### 3.4. Longitudinal Mass Transfer and Braking

The longitudinal mass transfer in the direction of the front tires results from the braking forces. Figure 14 shows the free-body diagram for this stress.

The maximum speed, the coefficient of friction between the tires and the asphalt, the position of the center of gravity, the braking time, and the weight of the vehicle are determined as initial conditions.

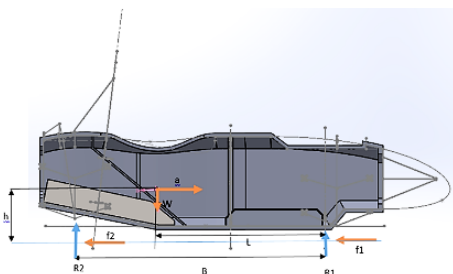


Figure 14. Longitudinal free-body diagram [15]

The calculated loads  $R1=1423.85$  N and  $f1=1181.79$  N involved in the longitudinal resistance and braking tests are taken as reference. However, in the simulation, all values are increased to further stress the model.

### 3.5. Side Impact Case

In the initial assessment, the vehicle's speed is assumed to be 40 km/h, considering the worst-case scenario, and applying a force of 4.5 G during the impact. A vehicle weight of 220 kg and a driver weight of 75 kg are used for the calculation [15]. By applying the formula for final velocity, considering a final velocity of 11.11 m/s corresponding to an initial velocity starting from rest, plus the multiplication of the acceleration (which is the value to be determined) by the time of 0.3 s, a value of 37.03 m/s<sup>2</sup> is obtained. Using this acceleration value, the resulting force is calculated by multiplying the acceleration by the mass of 290 kg, resulting in 10 739.66 N. This force is used for the simulation of the side impact [16].

### 3.6. Model Preparation in ANSYS ACP

The ANSYS software provides the Composite PrePost (ACP) tool to facilitate the creation of the finite element model and access the results.

Real models constructed with composite materials consist of multiple layers and various materials. Consequently, it is crucial to meticulously prepare the FEM model by ensuring accurate layer orientations and proper material stacking [17].

Figure 15 shows the final model with the layers in ANSYS ACP.

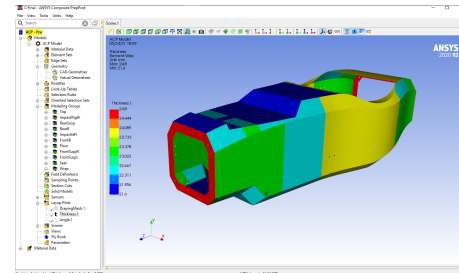


Figure 15. Final model in ANSYS ACP [15]

### 3.7. Analysis of the torsional rigidity of the model using FEM

Torsional rigidity is physically defined by the equation described below. Through FEM analysis, the total deformation is determined. Figure 16 shows how the values  $y1, x1$ . are measured [18].

$$k = \frac{M}{\theta}; \theta = \tan^{-1} \left( \frac{y1}{x1} \right)$$

Where:

M = Torsional moment (N\*m)

$\theta$  = Deformation angle (degrees)

$x1$  = Horizontal distance from the vehicle's central plane to the point where the deformation  $y1$  is measured.

$y1$  = Vertical deformation

$K$  = torsional rigidity (N\*m/degrees)

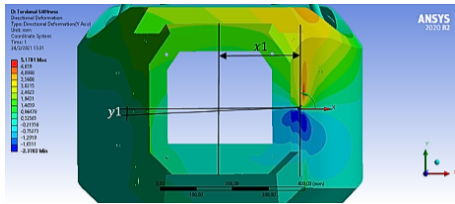


Figure 16. Distance  $x1$  and  $y1$  [15]

For this simulation, a force of 6870 N was applied, resulting in an average deformation of 1.001 mm and a maximum deformation of 4,2 mm as shown in Figure 17. A maximum deformation of 5,3 mm above the upper suspension point is observed where the stress is most concentrated.

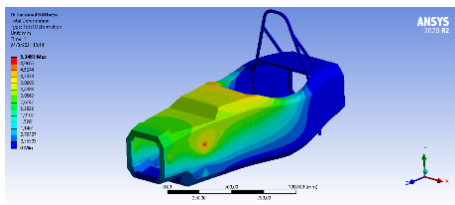


Figure 17. Torsional rigidity deformation [15]

### 3.8. Longitudinal rigidity analysis

To analyze this deformation, a load of 2500 N is applied to the front axle, resulting in a deformation of 1.99 mm, as shown in Figure 18.

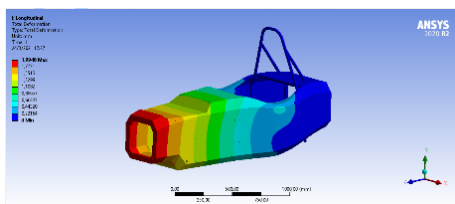


Figure 18. Longitudinal rigidity deformation [15]

Regarding the stress on the structure, the maximum value is 101.44 MPa, as shown in Figure 19. This stress is low because the structure exhibits a uniform distribution throughout its entirety.

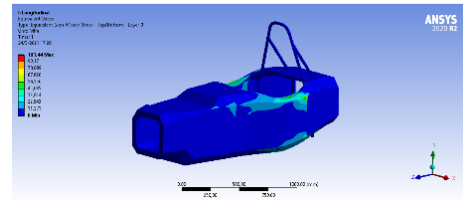


Figure 19. Longitudinal stresses [15]

### 3.9. Braking analysis

In this analysis, two loads are applied to the front axle with a value of 2500 N in the vertical direction and 2000 N in the longitudinal direction, resulting in a maximum deformation of 2.12 mm, as shown in Figure 20.

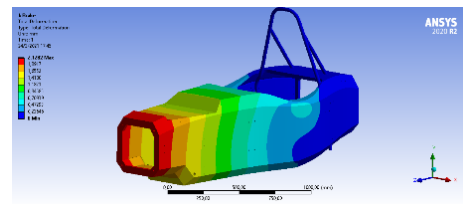


Figure 20. Braking deformation [15]

The maximum stress on the structure is 113.16 MPa, which does not cause material rupture, as shown in Figure 21.

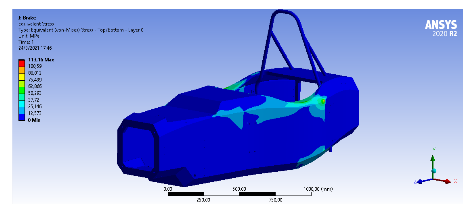


Figure 21. Braking stresses [15]

### 3.10. Side impact analysis

The value of this stress is 10,739.66 N, as detailed in section 3.53 [15]. The maximum deformation is 1.35 mm, as shown in Figure 22.

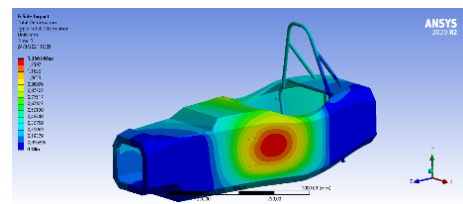


Figure 22. Side impact deformation [15]

The stress on the structure has a maximum value of 72.61 MPa, indicating a better distribution throughout the monocoque, as shown in Figure 23.

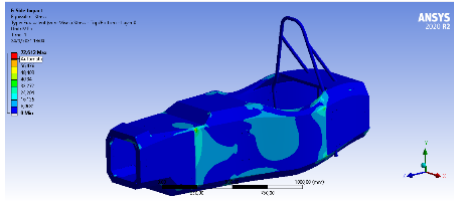


Figure 23. Side impact stresses [15]

### 3.11. Rollover simulation

In this simulation, three loads are applied: a longitudinal, a transverse, and a vertical load of 6 KN, 5 KN and 9 KN, respectively. The results show a maximum deformation value of 16.15 mm (Figure 24) and a maximum stress value of 426.52 MPa (Figure 25) [19].

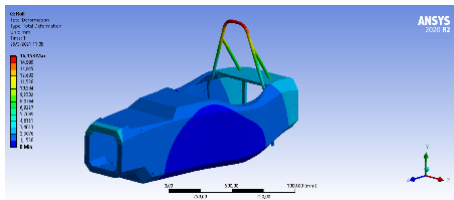


Figure 24. Main Hoop Deformation [15]

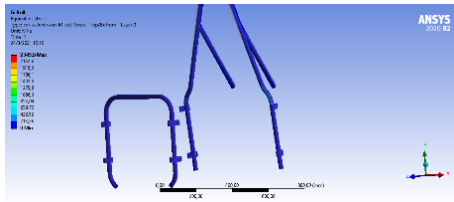


Figure 25. Main Hoop Stresses [15]

### 3.12. Weight simulation on the monocoque floor

In this simulation, the distributed weight of the elements is applied to the monocoque floor. Table 3 presents the weight of the elements and the corresponding forces exerted by them.

Table 3. Weight of the elements on the monocoque [15]

| Component | Weight (kg) | Force (N) |
|-----------|-------------|-----------|
| Driver    | 75          | 735.75    |
| Steering  | 12.5        | 122.62    |
| Battery   | 36          | 353.16    |
| Pedal box | 4.5         | 44.15     |
| Inverter  | 7           | 68.67     |

The results of this simulation show that the maximum deformation on the monocoque floor is 0.13 mm

(Figure 26), and the maximum stress is 15 MPa (Figure 27). This indicates that the material can perfectly withstand the weight of the elements.

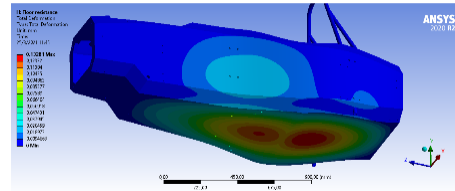


Figure 26. Floor deformation [15]

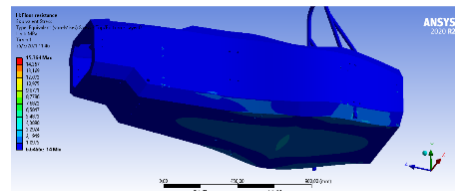


Figure 27. Floor stresses [15]

### 3.13. Data validation

#### 3.13.1. Design efficiency in terms of weight reduction

Considering the data obtained, an efficiency analysis was performed to assess the weight reduction of the prototype.

The EB17 model is used as a reference for comparison with the prototype design in this work [10].

Table 4 shows that the combined weight of the chassis and body is 55.31 kg, representing 23.54% of the total weight [15].

The material used in the Main and Front Hoop structures is "AISI 4130 steel normalized at 870 °C". The data were obtained from the EB17 simulation.

Figure 28 shows that using the software, a reduced weight of 0.0420 t (equivalent to 42 kg) was obtained without using the safety triangle in the ANSYS program. When adding the data from the safety triangle, the weight is 48.19 kg for the three combined elements [15]

Table 4. Approximate masses of EB17 [10]

| Component       | Mass (kg)  | %          |
|-----------------|------------|------------|
| Driver          | 80         | 33.75      |
| Engine          | 12         | 5.06       |
| Powertrain      | 20         | 8.43       |
| Steering system | 10         | 4.21       |
| Battery         | 80         | 33.75      |
| Chassis         | 35         | 14.76      |
| <b>Total</b>    | <b>237</b> | <b>100</b> |

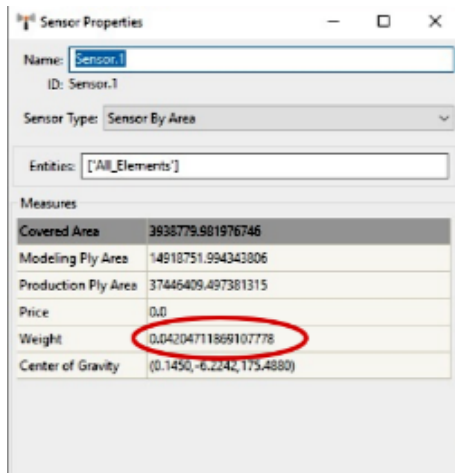


Figure 28. Preliminary weight of the monocoque obtained from ANSYS ACP [15]

For the final analysis, the weight of the monocoque was obtained by optimizing the layers of the model, as shown in Figure 29. Using its triangular structures, a weight of 0.0227 t (22.7 kg) was obtained, thus reducing nearly half of the initial weight.

Integrating safety elements increased security and reduced material layers, optimizing the weight. Along with its safety triangle, the final weight is 27.2 kg. The final weight optimization analysis shows a significant reduction compared to the EB17, which weighs 237 kg, with 55.31 kg resulting from the weight of the chassis and body. The monocoque has a final weight of 27.2 kg, indicating a 47.2% weight reduction optimization, which means 28.11 kg less for the theoretical single seater.

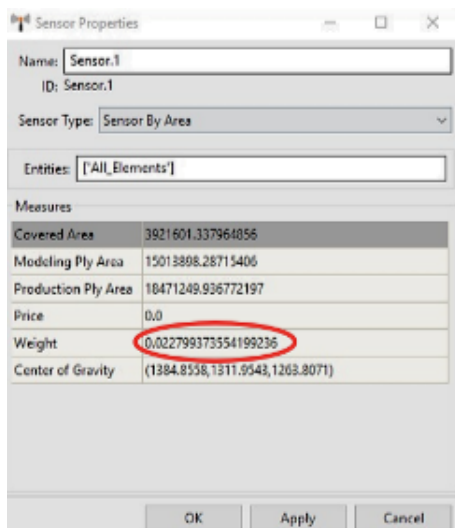


Figure 29. Final weight of the monocoque obtained from ANSYS ACP [15]

### 3.13.2. Torsional rigidity comparison

The monocoque demonstrates a superior stress dissipation capability, 2.1 times higher compared to the EB17 model, while also exhibiting a 17% reduction in stress concentration. Additionally, the monocoque boasts a 75% higher K value, which defines its torsional rigidity, in comparison to the EB17. This enhanced rigidity significantly contributes to the vehicle’s stability during cornering maneuvers. (Figure 30 and Table 5).

Table 5. Torsional rigidity of the models [15]

| Model     | Load (N) | Maximum stress | Maximum deformation | K (KNm/degree) |
|-----------|----------|----------------|---------------------|----------------|
| Monocoque | 6780     | 306.22 MPa     | 4.2 mm              | 30             |
| EB17      | 3133     | 370 MPa        | 3.8 mm              | 7.7            |

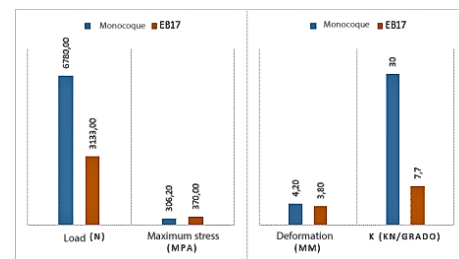


Figure 30. Torsional rigidity results [15]

### 3.13.3. Longitudinal rigidity comparison

The monocoque demonstrates an 11% reduction in applied load during the simulation, resulting in improved stress dissipation. This is attributed to a 45% decrease in stress concentration and a 50% reduction in deformation compared to the EB17 model. (Figure 31 and Table 6).

Table 6. Longitudinal rigidity comparison [15]

| Model     | Load (N) | Maximum stress | Maximum deformation |
|-----------|----------|----------------|---------------------|
| Monocoque | 2500     | 101.44 MPa     | 1.99 mm             |
| EB17      | 2782.68  | 182 MPa        | 4 mm                |

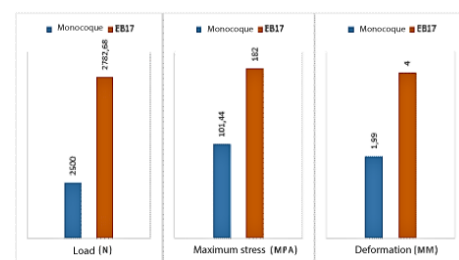


Figure 31. Longitudinal rigidity results [15]

### 3.13.4. Braking comparison

For this analysis, the loads acting on the front wheels are considered, including vertical and longitudinal loads on the vehicle. (Figure 32 and Table 7).

**Table 7.** Braking analysis [15]

| Model     | Vertical load | Longitudinal load | Maximum stress | Maximum deformation |
|-----------|---------------|-------------------|----------------|---------------------|
| Monocoque | 2500 N        | 2000 N            | 113.16 MPa     | 2.12 mm             |
| EB17      | 2782.68 N     | 2309.63 N         | 201 MPa        | 4.2 mm              |

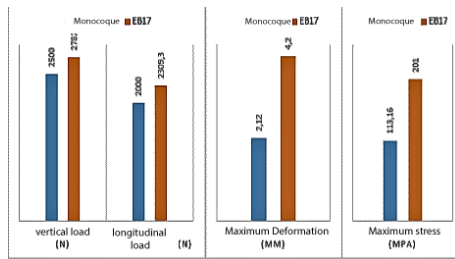


**Figure 32.** Braking results [15]

### 3.13.5. Side impact comparison

The monocoque experiences a reduction of 11% in vertical load and 14% in longitudinal load. This results in higher stress dissipation in the monocoque, as it exhibits a 44% reduction in stress concentration compared to the EB17. Additionally, the monocoque demonstrates a 44% decrease in deformation compared to the EB17 model. (Figure 33 and Table 8).

**Table 8.** Side impact analysis [15]

| Model     | Load (N) | Maximum stress | Maximum deformation |
|-----------|----------|----------------|---------------------|
| Monocoque | 10740    | 72.61 MPa      | 1.35 mm             |
| EB17      | 7000     | 361 MPa        | 3.32 mm             |

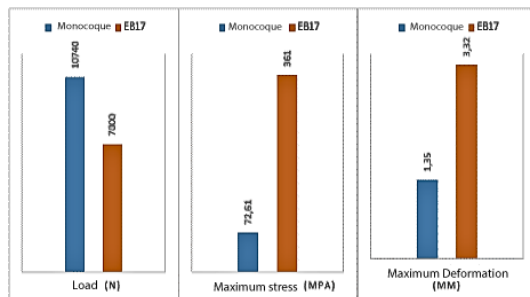


**Figure 33.** Side impact results [15]

The monocoque demonstrates superior stress dissipation within its structure, with a load 53% higher than that of the EB17 model and an 80% reduction

in stress accumulation. Furthermore, the monocoque exhibits a 60% decrease in deformation compared to its predecessor model.

## 4. Conclusions

Through the development of this article, the design proposal for a carbon fiber monocoque for a Formula Student single-seater has been determined. SolidWorks software has been used for modelling, and ANSYS software for simulation, allowing a thorough analysis of the performance and characteristics of the monocoque.

The proposal to use a monocoque chassis has achieved a weight reduction of 47.2% compared to its predecessor, the EB17, which had a tubular chassis. This demonstrates the superiority and relevance of implementing carbon fiber technology.

The proposed design implemented a sandwich structure utilizing ANSYS software. This structure enables the utilization of woven carbon fiber and aluminum Honeycomb. These materials have demonstrated excellent safety levels, and minimal deformations, and have successfully met safety standards.

## References

- [1] K. P. Hammer, *Design and Analysis of a Composite Monocoque for Structural Performance: A Comprehensive Approach*. Indiana University–Purdue University, 2019. [Online]. Available: <http://dx.doi.org/10.7912/C2/2703>
- [2] G. Davies, *Materials for automobile Bodies*. Elsevier, 2003. [Online]. Available: <https://bit.ly/42DnE9K>
- [3] Panel Systems. (2023) Larcore aluminium honeycomb panels. Panel Systems Ltda. [Online]. Available: <https://bit.ly/41F5dQs>
- [4] M. F. Ashby, *Materials Selection in Mechanical Design*. Butterworth-Heinemann, 2016. [Online]. Available: <https://bit.ly/41ETGAV>
- [5] F. P. Carballo, *Introducción al análisis y diseño con materiales compuestos*. Universidad de Sevilla, Escuela Técnica Superior de Ingenieros, 2008. [Online]. Available: <https://bit.ly/41z45hu>
- [6] C. A. Eurenium, N. Danielsson, A. Khokar, E. Krane, M. Olofsson, and J. Wass, *Analysis of Composite Chassis*. The Department of Applied Mechanics, Chalmers University of Technology, 2013. [Online]. Available: <https://bit.ly/3o38oE6>
- [7] F. Jourdan, *Degree Course in Automotive Engineering*. Politecnico di Torino, 2019. [Online]. Available: <https://bit.ly/3nZtHqb>

- [8] W. B. Riley and A. R. George, "Design, analysis and testing of a formula sae car chassis," in *Motorsports Engineering Conference & Exhibition*. SAE International, dec 2002. [Online]. Available: <https://doi.org/10.4271/2002-01-3300>
- [9] E. Tsirogiannis, G. Stavroulakis, and S. Makridis, "Design and modelling methodologies of an efficient and lightweight carbon-fiber reinforced epoxy monocoque chassis, suitable for an electric car," *Material Science and Engineering with Advanced Research*, vol. 2, pp. 5–12, 02 2017. [Online]. Available: <http://dx.doi.org/10.24218/msear.2017.21>
- [10] V. R. Álvarez Salazar, *Diseño y construcción de un chasis tubular de un vehículo de competencia Formula SAE eléctrico*. Universidad Politécnica Salesiana, 2018. [Online]. Available: <https://bit.ly/4324j1U>
- [11] SAE, *The 2020 Formula SAE Rules Version 1.0 are now published online under the Series Resources*. SAE International Privacy Policy, 2019. [Online]. Available: <https://bit.ly/4539Irb>
- [12] W. Contreras, P. Quezada, and L. Ortiz, *Propuesta metodológica para el diseño del chasis de un kart tipo KF4*. La ingeniería automotriz clave para el desarrollo sostenible de Ecuador, 2018, ch. Diseño Automotriz, pp. 55–77. [Online]. Available: <https://bit.ly/42EhUN2>
- [13] K. Egger, B. Ford, K. Nagao, N. Sharma, and D. Zusalim, *Formula SAE Monocoque Chassis Development*. Mechanical Engineering Department. California Polytechnic State University, San Luis Obispo, 2020. [Online]. Available: <https://bit.ly/42EiIl2>
- [14] J. Wu, O. Agyeman Badu, Y. Tai, and A. R. George, "Design, analysis, and simulation of an automotive carbon fiber monocoque chassis," *SAE International Journal of Passenger Cars - Mechanical Systems*, vol. 7, no. 2, pp. 838–861, apr 2014. [Online]. Available: <https://doi.org/10.4271/2014-01-1052>
- [15] C. A. Jaramillo Andrade and E. J. Pizarro Barrera, *Análisis y simulación de un monocasco de fibra de carbono para un monoplaza Formula Student*. Universidad Politécnica Salesiana, 2021. [Online]. Available: <https://bit.ly/3pFmc85>
- [16] R. Patil, "Fea analysis of fsae chassis," *International Journal of Engineering Research and*, vol. V9, 07 2020. [Online]. Available: <http://dx.doi.org/10.17577/IJERTV9IS070148>
- [17] B. Zhao, *Analysis of composite plates by using mechanics of structure genome and comparison with ANSYS*. Aeronautics and Astronautics. Purdue University Indianapolis, 2016. [Online]. Available: <https://bit.ly/3pQw8LW>
- [18] F. P. Ruiz and M. Solís Muñiz, *Diseño y cálculo del chasis monocasco de un monoplaza de competición tipo fórmula*. Tesis de Grado. Ingeniería Industrial. Escuela Técnica Superior de Ingeniería. Universidad de Sevilla. España, 2016. [Online]. Available: <https://bit.ly/3o8NT91>
- [19] M. Tamjidillah, R. Subagyo, H. Isworo, and H. Y. Nanlohy, "Modelling analysis of high effect of roll hoop main on the strength of student car formula chassis," *Journal of Achievements in Materials and Manufacturing Engineering*, vol. 1, pp. 26–40, 05 2020. [Online]. Available: <http://dx.doi.org/10.5604/01.3001.0014.1959>